Stability analysis and design of steel-concrete composite columns

M. D. Denavit[1], J. F. Hajjar[2], R. T. Leon[3]

Abstract
This paper investigates the use of the Direct Analysis method, established within the AISC *Specification for Structural Steel Buildings*, for steel-concrete composite beam-columns, including both concrete-filled steel tube and steel reinforced concrete members. In addition, the paper outlines recommendations for equivalent flexural rigidity to be used in elastic analyses for composite columns. Both the Direct Analysis recommendations and equivalent rigidity values were developed based on computational results from a comprehensive suite of analyses of benchmark frames. The validity of the elastic analysis and design approach is confirmed though comparisons to results of fully nonlinear analyses using distributed plasticity finite elements that explicitly model the key phenomena that affect system response, including member inelasticity (e.g., concrete cracking and steel residual stresses) and initial geometric imperfections.

1. Introduction
Composite frames have been shown to be an effective option for use as the primary lateral force resistance system of building structures; and in many cases offer significant advantages over other lateral force resistance systems (Hajjar 2002). However, little guidance is available regarding the value of flexural rigidity that should be used in elastic analyses of complete composite frames. In addition, no comprehensive validation has been conducted for the use of the Direct Analysis method (AISC 2010b) with composite structures. This paper presents work conducted as part of a NEES research project to build core knowledge on the behavior of composite beam-columns and to develop rational stability analysis and design recommendations for both non-seismic and seismic loading.

The Direct Analysis method provides a straightforward and accurate way of addressing frame in-plane stability considerations (White et al. 2006). In this method, required strengths are determined with a second-order elastic analysis where members are modeled with a reduced rigidity and initial imperfections are either directly modeled or represented with notional lateral loads. The method allows for the computation of available strength based on the unsupported length of the column, eliminating the need to compute an effective length factor. The validity of

---

[1] Graduate Research Assistant, University of Illinois at Urbana-Champaign, <denavit2@illinois.edu>
[2] Professor and Chair, Northeastern University, <jf.hajjar@neu.edu>
[3] David H. Burrows Professor of Construction Engineering, Virginia Polytechnic Institute and State University, <rleon@vt.edu>

this approach has been established through comparisons between fully nonlinear analyses and elastic analyses (Surovek-Maleck and White 2004a; b; Deierlein 2003; Martinez-Garcia 2002). However, to date, no appropriate reduced elastic rigidity values have been developed nor has the methodology in general been thoroughly validated for composite members.

Among the challenges to validation of the Direct Analysis method for composite members is the lack of guidance on the value of elastic flexural rigidity (EI) that should be used for analysis of composite members. An estimation of the flexural rigidity is necessary for first- and second-order static and dynamic analyses, as well as eigenvalue analyses. When used for this purpose the flexural rigidity is denoted as $EI_{elastic}$. Such a value could be used: 1) in conjunction with Direct Analysis rigidity reductions to perform strength checks; 2) to compute story drifts used in interstory drift checks; 3) to compute fundamental periods and mode shapes (including for response spectrum analysis); and 4) as the elastic component of a concentrated plasticity beam-column element.

The elastic flexural rigidity is also used in the determination of the elastic critical buckling load when computing axial compressive strength. When used for this purpose the flexural rigidity is denoted as EI_{eff}. The AISC *Specification* provides expressions for EI_{eff} for steel reinforced concrete (SRC) columns (Eq. 1) for concrete-filled steel tube (CFT) columns (Eq. 3) based on an examination of experimental research (Leon et al. 2007).

$$EI_{eff} = E_s I_s + 0.5 E_s I_{sr} + C_1 E_c I_c \qquad \text{(SRC)} \qquad (1)$$

$$C_1 = 0.1 + 2\left(\frac{A_s}{A_c + A_s}\right) \leq 0.3 \qquad (2)$$

$$EI_{eff} = E_s I_s + E_s I_{sr} + C_3 E_c I_c \qquad \text{(CFT)} \qquad (3)$$

$$C_3 = 0.6 + 2\left(\frac{A_s}{A_c + A_s}\right) \leq 0.9 \qquad (4)$$

Since concrete experiences nonlinearity a relatively low load levels, one value or expression for the elastic rigidity is generally insufficient. For example, EI_{eff} should be representative of axial dominant behavior near incipient buckling whereas it may be more appropriate for $EI_{elastic}$ used to determine story drift to be representative of combined axial and bending behavior at lower load levels. This is in contrast to structural steel where $EI_{eff} = EI_{elastic} = E_s I_s$ is widely considered safe and accurate for nearly all of these purposes as they relate to common design procedures.

In order to address these current needs in design, a large parametric study has been conducted. The study focuses on two related aspects of stability design. First is the development of an effective elastic rigidity, $EI_{elastic}$, for use in frame analyses with composite beam-columns. Second is the development and validation of Direct Analysis recommendations for stability design of composite systems.

2. Benchmark Frames
The parametric study described in this work generally consists of comparisons between results from fully nonlinear analyses and elastic analyses on a set of benchmark frames. In order to ensure broad applicability of the recommendations, the benchmark frames are selected to cover a wide range of material and geometric properties. Similar studies for structural steel (Kanchanalai 1977; Surovek-Maleck and White 2004a; b) have used a set of small non-redundant frames and a W8×31 section in both strong and weak axis. For this work, this set of frames was expanded and a variety of composite cross sections were selected. In the parametric study, a complete matrix is laid out whereby each cross section is used within each benchmark frame to provide a comprehensive set of results.

2.1 Sections
The cross sections chosen for investigation in this work are segregated into four groups 1) Circular CFT (CCFT), 2) Rectangular CFT (RCFT), 3) SRC subjected to strong axis bending, and 4) SRC subjected to weak axis bending. Within these groups, sections were selected to span practical ranges of concrete strength, steel ratio, and for the SRC sections, reinforcing ratio (only CFTs without longitudinal reinforcing bars are analyzed in this work). Other section properties (e.g., steel yield stress, aspect ratio) were taken as typical values. Steel yield strengths were selected as F_y = 50 ksi for W shapes, F_y = 42 ksi for round HSS shapes, F_y = 46 ksi for rectangular HSS shapes, and F_{yr} = 60 ksi for reinforcing bars. Three concrete strengths were selected: 4, 8, and 16 ksi.

There is no prescribed upper limit of steel ratio for composite sections; however, practical considerations and the dimensions commonly produced steel shapes impose an upper limit of approximately 25% for CFT and 12% for SRC. The AISC *Specification* sets a lower limit of steel ratio for composite sections as 1%. However, maximum permitted width-to-thickness ratios provide a stricter limit for CFT members. For the selected steel strengths, the width-to-thickness limits (Eq. 5) correspond to steel ratio limits of 1.86% for CCFT and 3.16% for RCFT. For SRC members, the AISC *Specification* prescribes a minimum reinforcing ratio of 0.4% and no maximum. The ACI *Code* prescribes a maximum reinforcing ratio of 8%.

$$\frac{D}{t} \leq \frac{0.31E_s}{F_y} \qquad \text{(CCFT)}$$

$$\frac{h}{t} \leq 5.00 \sqrt{\frac{E_s}{F_y}} \qquad \text{(RCFT)}$$

(5)

Noting these limitations 5 round HSS shapes were selected for the CCFT sections, 5 rectangular HSS shapes were selected for the RCFT sections, and outside dimensions of 28 in. × 28 in., 4 wide-flange shapes, and 3 reinforcing configurations were selected for the SRC sections (Table 1). Altogether, 5 (steel shapes) × 3 (concrete strengths) = 15 total sections were selected each for RCFTs and CCFTs and 4 (steel shapes) × 3 (reinforcing configurations) × 3 (concrete strengths) = 36 total sections were selected each for strong and weak axis bending of SRCs.

Table 1: Selected steel shapes and reinforcing configurations

Index	Steel Shape	ρ_s		Index	Steel Shape	ρ_s
A	HSS 7.000×0.500	24.82%		A	HSS 6×6×1/2	27.63%
B	HSS 10.000×0.500	17.70%		B	HSS 9×9×1/2	19.06%
C	HSS 12.750×0.375	10.65%		C	HSS 8×8×1/4	11.13%
D	HSS 16.000×0.250	5.72%		D	HSS 9×9×1/8	5.05%
E	HSS 24.000×0.125[*]	1.93%		E	HSS 14×14×1/8[*]	3.27%

* Not in the AISC *Manual*   * Not in the AISC *Manual*

(a) CCFT   (b) RCFT

Index	Steel Shape	ρ_s		Index	Reinforcing	ρ_{sr}
A	W14×311	11.66%		A	20 #11	3.98%
B	W14×233	8.74%		B	12 #10	1.94%
C	W12×120	4.49%		C	4 #8	0.40%
D	W8×31	1.16%				

(c) SRC (steel shapes)   (d) SRC (reinforcing configurations)

2.2 Frames

A set of 23 small non-redundant frames were described and used in previous stability studies on structural steel members (Kanchanalai 1977; Surovek-Maleck and White 2004a; b). The set includes both sidesway inhibited and sidesway uninhibited frames, a range of slenderness, end constraints, and leaning column loads. The set of frames was expanded and the frame parameters were generalized for use with composite sections in this study. The frames are shown schematically in Figure 1. The sidesway uninhibited frame is defined by a slenderness value, λ_{oe1g}, pair of end restraint parameters, $G_{g,top}$ and $G_{g,bot}$, and leaning column load ratio, γ. The sidesway inhibited frame is defined by a slenderness value, λ_{oe1g}, and end moment ratio, β. The values of these parameters selected for the frames are described in Table 2, a total of 84 frames are selected. The "g" in the end restraint parameters and slenderness value denotes that these values are defined with respect to gross section properties.
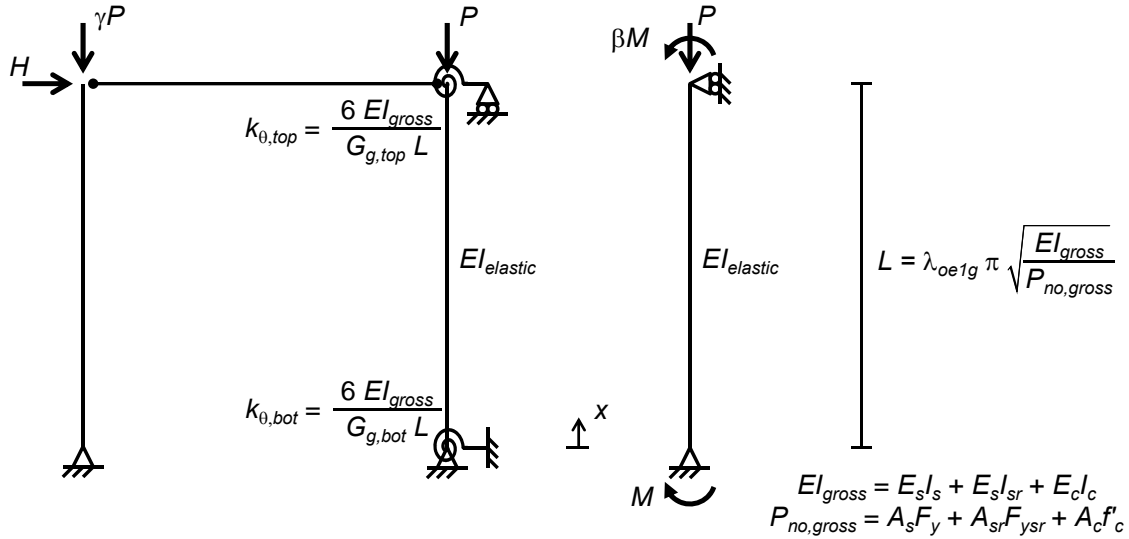

Figure 1: Schematic of the benchmark frames

Frame	Slenderness	End Restraint	Leaning Column Load Ratio	End Moment Ratio	Number of Frames
Sidesway Uninhibited	4 values λ_{oelg} = {0.22, 0.45, 0.67, 0.90}	4 value pairs (Table 3)	4 values γ = {0, 1, 2, 3}	n/a	64 (= 4 × 4 × 4)
Sidesway Inhibited	4 values λ_{oelg} = {0.45, 0.90, 1.35, 1.90}	n/a	n/a	5 values β = {–1.0, –0.5, 0.0, 0.5, 1.0}	20 (= 4 × 5)

Table 3: End Restraint Value Pairs

Pair	$G_{g,top}$	$G_{g,bot}$
A	0	0
B	1 or 3*	1 or 3*
C	0	∞
D	1 or 3*	∞

*3 when γ = 0; 1 otherwise

2.3 Second-Order Elastic Analysis of Benchmark Frames

The second-order elastic results described in this work were obtained from the solution of the governing differential equation (Eq. 6) using the appropriate boundary conditions (Table 4). Closed form solutions were obtained for displacement and moment along the length of column using a computer algebra system. This approach is computationally quick and accurate for moderate displacements; however, axial deformations are neglected. Where necessary, the effective length factor, *K*, for the benchmark frames was computed using the same differential equation.

$$v''''(x) + \sqrt{\frac{P}{EI_{elastic}}}v''(x) = 0 \tag{6}$$

Table 4: Boundary conditions for the benchmark frames

Boundary Condition	Sidesway Uninhibited	Sidesway Inhibited
1	$v(0) = 0$	$v(0) = 0$
2	$-EI_{elastic}v''(0) = -k_{\theta bot}v'(0)$	$-EI_{elastic}v''(0) = M$
3	$-EI_{elastic}v'''(L) - Pv'(L) = H + \frac{\gamma P}{L}v(L)$	$v(L) = 0$
4	$-EI_{elastic}v''(L) = k_{\theta top}v'(L)$	$-EI_{elastic}v''(L) = \beta M$

3. Fully Nonlinear Analysis of Benchmark Frames

In order to provide validated results against which the proposed elastic design methodologies may be evaluated, a fully nonlinear analysis formulation is used for both CFT and SRC beam-columns that has been validated extensively against experiments for both monotonic and cyclic loading. This section outlines details of the nonlinear formulation.

3.1 Mixed Beam Finite Element Formulation

A mixed beam finite element formulation for composite members has been developed and extensively validated against experimental results in prior research (Tort and Hajjar 2010; Denavit and Hajjar 2012; Denavit et al. 2011). Among the results against which the formulation was validated was a set of full-scale slender beam-columns subjected to complex three-dimensional loading (axial compression plus biaxial bending moment) performed as part of this project (Perea 2010). The formulation is implemented in the OpenSees framework (McKenna et al. 2000) and was used to perform the fully nonlinear analyses described in this work. It is a Total Lagrangian formulation assuming small strains and moderate rotations in the corotational frame and coupled with an accurate geometric transformation. With multiple elements along the length of a column, large displacement and rotation behavior is captured accurately. The constitutive relations were simplified for this study to better correspond to assumptions common in the development of design recommendations (e.g., neglecting steel hardening and concrete tension strength). Local buckling of the steel tube and other steel components was neglected in the fully nonlinear analyses. This simplification allows for the investigation of the full range of steel ratios without the complexity of modeling local buckling, and is consistent with the validations conducted when developing Direct Analysis for steel structures (Surovek-Maleck and White 2004a; b). It is thus assumed that when combined with existing local buckling provisions in the AISC *Specification*, the proposed design provisions are applicable to composite members with non-compact or slender sections.
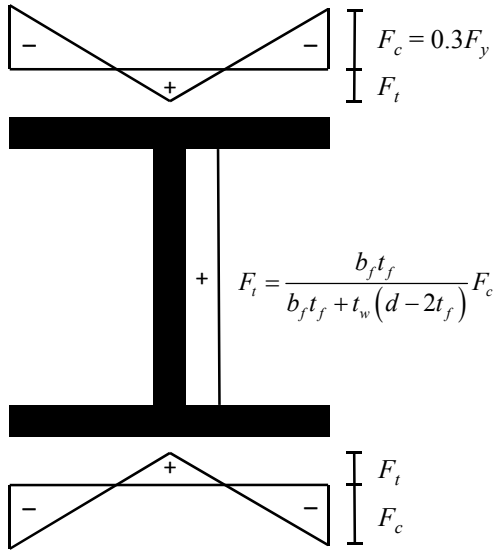
As in the prior work on the Direct Analysis method (Surovek-Maleck and White 2004b) wide-flange shapes are modeled with elastic-perfectly plastic constitutive relations (Figure 2c) and the Lehigh residual stress pattern (Galambos and Ketter 1959) (Figure 2a). Reinforcing steel was assumed to have negligible residual stress and was also modeled with an elastic-perfectly plastic constitutive relation. Residual stresses in cold formed steel tubes vary through thickness. To allow a reasonable fiber discretization of the CFT sections, residual stresses are included implicitly in the constitutive relation. A multilinear constitutive relation (Figure 2b) was used in which the stiffness decreases at 75% of the yield stress and again at 87.5% of the yield stress to approximate the gradual transition into plasticity observed in cold-formed steel (Abdel-Rahman and Sivakumaran 1997). In addition, the yield stress in the corner region of the rectangular members is increased to account for the additional work hardening in that region (Abdel-Rahman and Sivakumaran 1997).

The Popovics concrete model (Figure 2d) was selected because it allows for the explicit definition of the initial modulus, peak stress, and strain at peak stress. The modulus of elasticity of concrete is given by Eq. 7, this is equivalent to expression in the ACI *Code* for normalweight concrete and to the expression in the AISC *Specification* for w_c = 148.1 lbs/ft³. For RCFTs, the peak stress was taken as f'_c (Tort and Hajjar 2010). For CCFTs, the peak stress was increased to account the confinement provided by the steel tube using the model described by Denavit and Hajjar (2012). For SRCs, the concrete was divided into three regions: concrete cover, moderately confined concrete, and highly confined concrete, and the peak stress was computed for each region using the model described by Denavit et al. (2011). The strain at peak stress is given by Eq. 8 for unconfined concrete and Eq. 9 for confined concrete based on recommendations by Chang and Mander (1994).
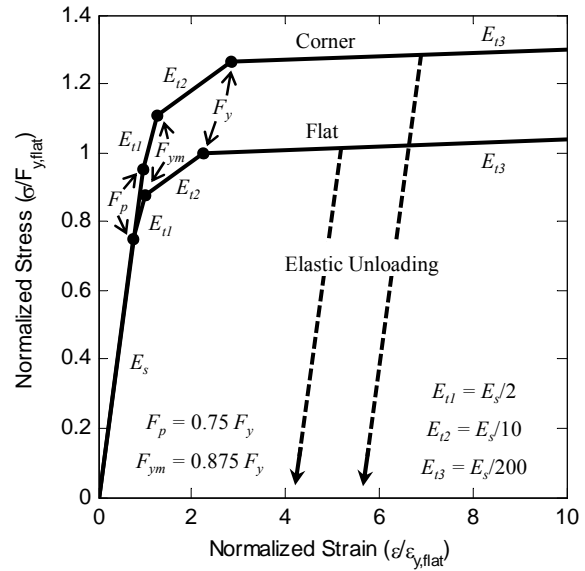
$$E_c\left[\text{ksi}\right] = 1802\sqrt{f'_c\left[\text{ksi}\right]} \tag{7}$$

$$\varepsilon_c = \frac{f'_c\left[\text{ksi}\right]^{1/4}}{710} \tag{8}$$

$$\varepsilon_{cc} = \varepsilon_c\left(1 + 5\left(\frac{f'_{cc}}{f'_c} - 1\right)\right) \tag{9}$$
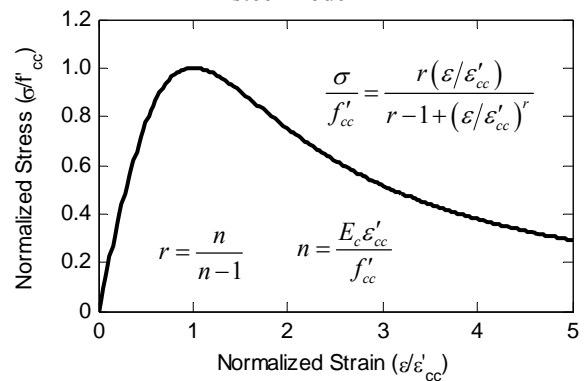
$F_c = 0.3F_y$

F_t

$F_t = \dfrac{b_f t_f}{b_f t_f + t_w\left(d - 2t_f\right)} F_c$

F_t

F_c

(a) Lehigh residual stress pattern

(b) Abdel-Rahman and Sivakumaran cold formed steel model

$F_p = 0.75\,F_y$

$F_{ym} = 0.875\,F_y$

$E_{t1} = E_s/2$

$E_{t2} = E_s/10$

$E_{t3} = E_s/200$
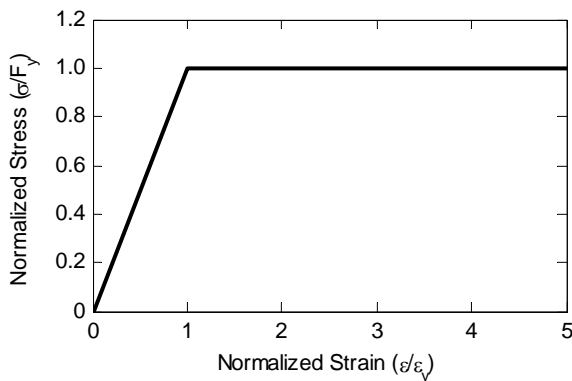
(c) Elastic-perfectly plastic model

(d) Popovics concrete model

$$\frac{\sigma}{f'_{cc}} = \frac{r\left(\varepsilon/\varepsilon'_{cc}\right)}{r - 1 + \left(\varepsilon/\varepsilon'_{cc}\right)^r}$$

$$r = \frac{n}{n-1} \qquad n = \frac{E_c \varepsilon'_{cc}}{f'_{cc}}$$

Figure 2: Steel and Concrete Constitutive Relations

All frame analyses were performed with six elements along the length of the member, each with three integration points. Since the analyses were two-dimensional, strips were used for the fiber section; the nominal height of the strips was 1/30th of the section depth (e.g., for a CCFT section, approximately 30 steel and 30 concrete strips of near equal height were used).

3.2 Initial Geometric Imperfections

Nominal geometric imperfections equal to the fabrication and erection tolerations in the AISC Code of Standard Practice (AISC 2010a) were modeled explicitly. An out-of-plumbness of $L/500$ was included for the sidesway uninhibited frames and a half sine wave out-of-straightness with maximum amplitude of $L/1000$ was included for all frames. The pattern of the initial geometric imperfections was applied to induce the greatest destabilizing effect.

3.3 Axial Compression-Bending Moment Interaction Diagrams

Through a series of fully nonlinear analyses, axial compression-bending moment interaction diagrams for each section and frame were constructed. One analysis was performed with axial load only to obtain the critical axial load, then a series analyses applying a constant axial load and increasing lateral load were performed. For the case of zero applied axial load, a cross section analysis was performed in lieu of the frame analysis. In each analysis, the limit point was identified as when the lowest eigenvalue reached zero; in cases where this did not occur, the limit point was defined as when the maximum longitudinal strain within any section in the member reached 0.05. At the limit point, both the applied loads and internal forces were recorded allowing for the construction of the first-order applied load interaction diagram and the second-order internal force interaction diagram, respectively. A sample of the results for two RCFT sections [RCFT-B-4 (ρ_s = 19.06%, f'_c = 4 ksi) and RCFT-E-4 (ρ_s = 3.27%, f'_c = 4 ksi)] and one frame [UA-67-g1 (sidesway uninhibited, fixed-fixed, K=1, λ_{oeg} = 0.67, leaning column load ratio = 1)] is shown in Figure 3. These two sections and one frame were selected primarily to illustrate the methodology. While the results from these sections and frame are typical and show variation between members with high and low steel ratios, they are not representative of the wide range of material and geometric properties explored in this study.
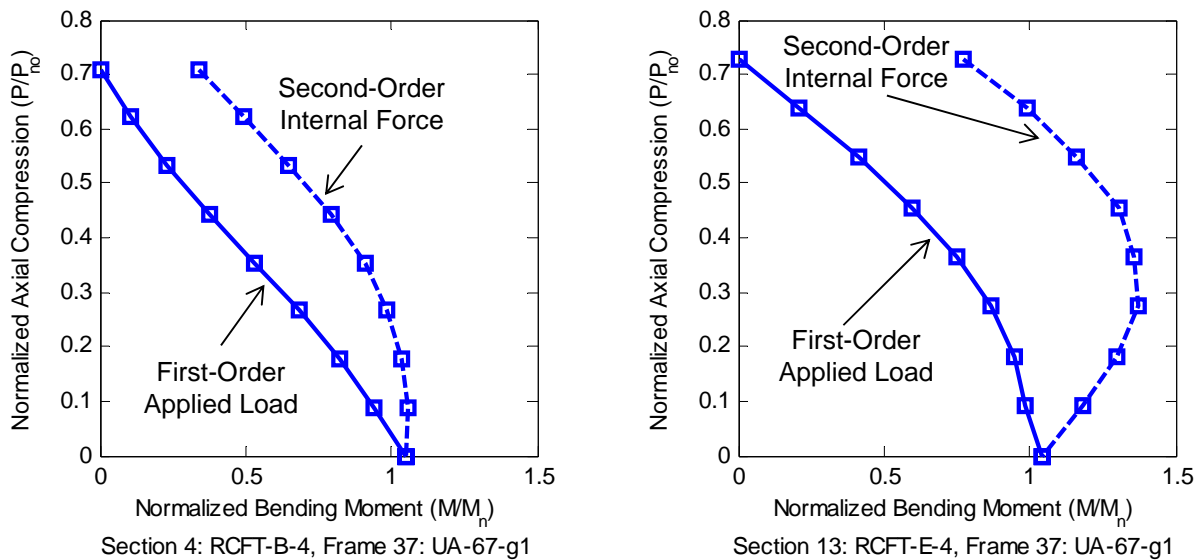

Section 4: RCFT-B-4, Frame 37: UA-67-g1   Section 13: RCFT-E-4, Frame 37: UA-67-g1

Figure 3: Example Results: Fully Nonlinear Applied Load and Internal Force Interaction Diagrams

4. Flexural Rigidity for Elastic Analyses

Because inelastic response in the concrete initiates at low load levels, an appropriate flexural rigidity for elastic analysis should be taken as a secant value. In order to assess the elastic flexural rigidity, $EI_{elastic}$, a parametric study was performed recording peak deformations from

inelastic analyses and determining the value of $EI_{elastic}$ that, when used in an elastic analysis, would result in the same peak deformations. One value of $EI_{elastic}$ was determined for each frame and section and for different pairs of applied axial load and moment.

The pairs of applied axial load and moment were selected to be evenly spaced within the applied load interaction computed as described above. Secondary fully nonlinear analyses were performed to obtain the target peak deformations. The secondary fully nonlinear analyses differ from the fully nonlinear analyses described previously in that no initial geometric imperfections were included and tension strength was included in the concrete constitutive relation, since for this study the average behavior rather than lower bound behavior is of interest. For each load pair, $EI_{elastic}$ was determined through an iterative process such that the peak deformation from the elastic analysis was equal to the target peak deformation. A sample of the results for the sections and frame shown previously is shown in Figure 4. Each of the points represents one applied axial load and moment pair, the color corresponds to the value of $EI_{elastic}$ that was obtained as described above, normalized with respect to the gross flexural rigidity.
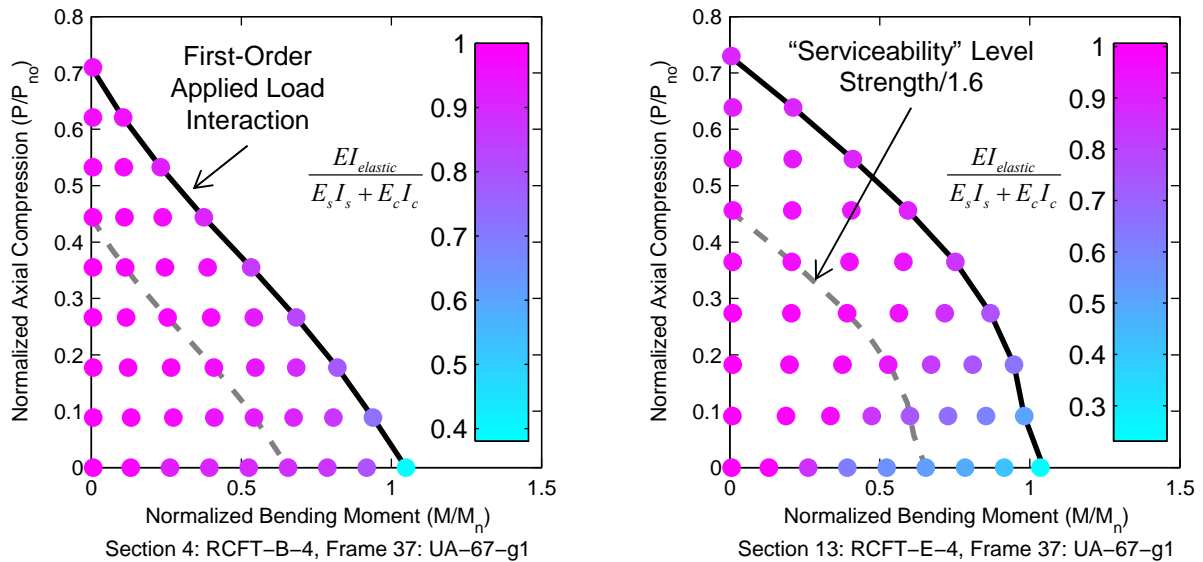

Figure 4: Example Results: $EI_{elastic}$

Figure 4 shows that the flexural rigidity varies with load level. At low loading, the gross flexural rigidity is a good estimate of the elastic rigidity ($EI_{elastic} \approx EI_{gross}$). As the load increases, the elastic rigidity decreases, with greater decreases for moment dominate loading and lesser decreases for axial dominant loading.

A linear regression analysis was performed on the data obtained in this study to build a formula for $EI_{elastic}$. The strongest variations in $EI_{elastic}$ and thus the most accurate formula depend on the loading. An example of such a formula for RCFTs based only on data at or below the serviceability load level (Figure 4) is given in Eqs. 10 and 11 (coefficient of determination = 0.71). Similar, load-dependent formulas have been developed for the flexural rigidity of reinforced concrete members (Khuntia and Ghosh 2004). Unfortunately, when $EI_{elastic}$ depends on the loading, the elastic analysis becomes iterative, making this type of formula cumbersome

for design. More practical alternatives are discussed later in the context of the Direct Analysis method.

$$EI_{elastic} = E_s I_s + C_4 E_c I_c \qquad \text{(RCFT)} \tag{10}$$

$$C_4 = 1.01 - 0.90 \frac{M}{M_n}\left(1 - 3.39\frac{P}{P_{no}}\right) \leq 1.00 \tag{11}$$

5. Axial Strength

In the AISC *Specification*, the same column curve is used to predict the nominal axial compressive strength for both structural steel and composite columns (Eq. 12), where the slenderness, λ_{oe}, is given by Eq. 13, the effective rigidity, EI_{eff}, is given by Eq. 1 for SRCs and by Eq. 3 for CFTs, and the nominal zero-length compressive strength, P_{no}, is given by Eq. 14 for SRCs and by Eq. 15 for CFTs ($C_2 = 0.85$ for RCFTs and $C_2 = 0.95$ for CCFTs), noting that in this study local buckling is neglected and only CFTs without longitudinal reinforcement are investigated.

$$\frac{P_n}{P_{no}} = \begin{cases} 0.658^{\lambda_{oe}^2} & \text{for } \lambda_{oe} \leq 1.5 \\ 0.877/\lambda_{oe}^2 & \text{for } \lambda_{oe} > 1.5 \end{cases} \tag{12}$$

$$\lambda_{oe} = \frac{KL}{\pi}\sqrt{\frac{P_{no}}{EI_{eff}}} \tag{13}$$

$$P_{no} = F_y A_s + F_{ysr} A_{sr} + 0.85 f_c' A_c \qquad \text{(SRC)} \tag{14}$$

$$P_{no} = F_y A_s + C_2 f_c' A_c \qquad \text{(CFT)} \tag{15}$$

The critical axial load obtained from the fully nonlinear analyses, $P_{n,analysis}$, for each frame and section is compared to the design strength in Figure 5. For CFTs, the design axial strength is generally accurate. In the low and intermediate slenderness range ($\lambda_{oe}<2$), the axial compressive strength of concrete dominant sections (low values of ρ_s) tends to be underpredicted. However, the strength tends to be overpredicted for these sections in the high slenderness range ($\lambda_{oe}>2$) by as much as 15%. For CCFTs, the strength steel dominant sections in the intermediate slenderness range ($0.5<\lambda_{oe}<2$) is underpredicted by as much as 15%.

For SRCs, the design axial strength is inaccurate, underpredicting the strength by a significant margin, especially for concrete dominant sections. Based on these results, a new expression for the effective rigidity of SRC columns is presented (Eqs. 16-17). An alternative expression where $C_1 = 0.75$ for all sections was found to be accurate for axially loaded columns but is not recommended because it performed poorly when used to compute beam-column strength due to the concavity of the applied load interaction diagrams as described later. A comparison between the critical axial load obtained from the fully nonlinear analyses and the strength computed using the proposed expression is shown in Figure 6.
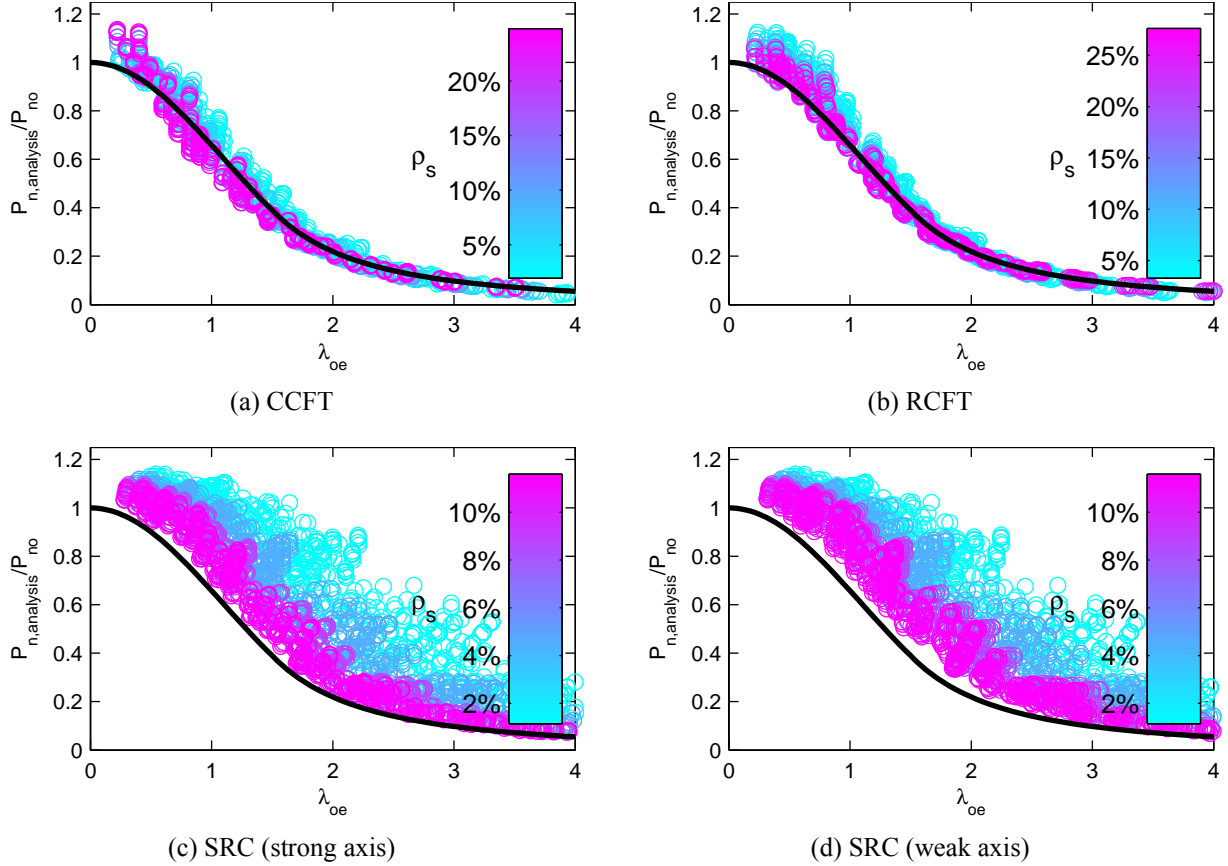
(a) CCFT   (b) RCFT

(c) SRC (strong axis)   (d) SRC (weak axis)

Figure 5: Comparison of Axial Strength: AISC 2010

$$EI_{eff,proposed} = E_s I_s + E_s I_{sr} + C_{1,proposed} E_c I_c \qquad \text{(SRC)} \qquad (16)$$

$$C_{1,proposed} = 0.60 + \frac{2A_s}{A_g} \le 0.75 \qquad (17)$$

The values of EI_{eff} computed with the proposed equation (Eq. 16) will be larger than those computed with the existing equation (Eq. 1), resulting in larger axial compressive strengths as seen in Figure 6a and b compared to Figure 5c and d. In order to verify the accuracy of this new formula, a comparison is made with concentrically loaded SRC columns experiments. Axial compressive strengths of a representative subset (Anslijn and Janss 1974; Chen et al. 1992; Han and Kim 1995; Han et al. 1992; Roderick and Loke 1975) of the database used in the original calibration of C_1 (Leon et al. 2007) were computed using the proposed formulas (Eqs. 12-14 and 16-17) and compared against the experimental axial compressive strengths in Figure 7. For this set of 52 columns (which fail predominantly about the weak axis), the section depths range from 6.3 in. to 14 in., concrete strengths range from 2.9 ksi to 9.5 ksi, measured steel yield strengths range from 39 ksi to 73 ksi, and the length-to-depth ratios range from 3.1 to 17.8; see Leon et al. (2007) for the geometric, material, and boundary condition details of these experiments. The computed axial strength compares well for a majority of the tests, although some fall below the column curve. The current resistance factor and safety factors ($\phi_c = 0.75$ and $\Omega_c = 2.00$) were

found to be suitable and somewhat conservative with the proposed formulas following the recommendations by Ravindra and Galambos (1978) and a reliability index of 3.0.
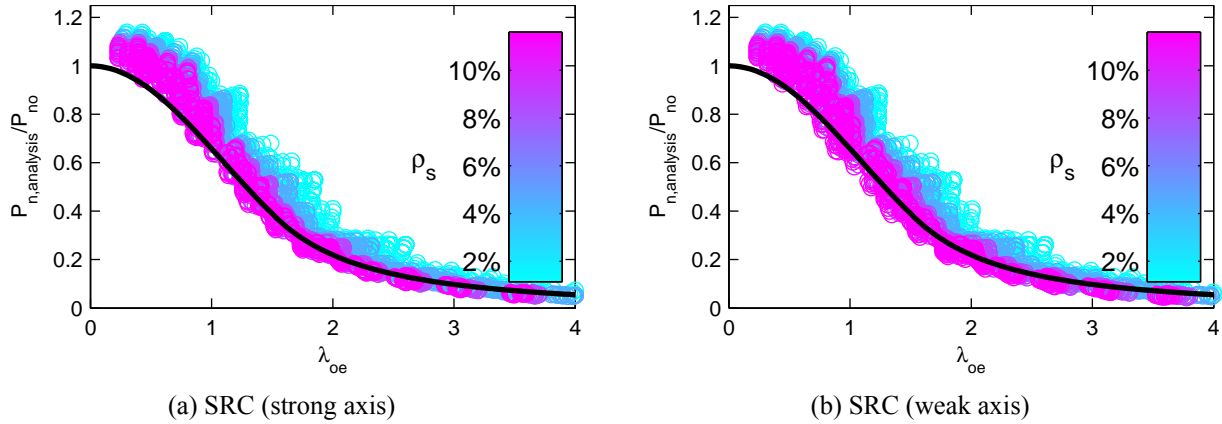

(a) SRC (strong axis)   (b) SRC (weak axis)

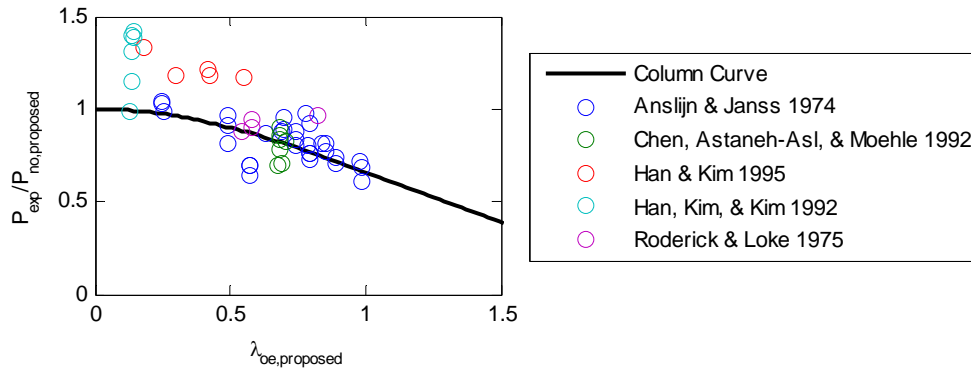Figure 6: Comparison of Axial Strength: Proposed

Figure 7: Comparison of Experimental Axial Strength: Proposed

6. Direct Analysis

Cross section strength curves for composite members are quite convex, especially for concrete dominant members. Beam-column strength curves are much less convex (and often concave) due to the fact that material nonlinearity (primarily concrete cracking but also concrete crushing and steel yielding) initiates at low load levels and severely reduces flexural rigidity. This effect is greater for more slender columns since the second order effects are greater but also because the ratio of bending moment to axial load is greater, a condition which leads to greater reductions in effective slenderness (as seen in Section 4). For design methodologies in which the effective slenderness of the member is computed, it is possible for this variation to be accounted for directly in the shape of the design interaction diagram. For the Direct Analysis method, the effective slenderness is never computed, as the unsupported length of the member is used instead. Thus, unless the concave shape is accounted for otherwise, the strength of members with high effective length factors will be overestimated. Rigidity reductions that depend on both axial load and bending moment could potentially help account for the shape, but would be cumbersome in design. The proposed design methodology presented below accounts for these effects with modifications to the design interaction curve and is shown to be safe and accurate for all beam-columns with practical effective length factors ($K<3$). For beam-columns with large

effective length factors, the unconservative error can sometimes exceed 5%, particularly for concrete dominant sections.

6.1 Calculation of Required Strength

As prescribed in the Direct Analysis method, internal forces must be determined using a second-order elastic analysis with reduced elastic rigidity and consideration of initial imperfections. The reduced rigidity, EI_{DA}, for structural steel members is described by Eq. 18 where τ_b depends on the required axial strength, P_r (Eq. 19).

$$EI_{DA} = 0.8\tau_b EI_{elastic} \tag{18}$$

$$\tau_b = \begin{cases} 1.0 & \text{for } P_r/P_{no} \leq 0.5 \\ 4\left(P_r/P_{no}\right)\left(1 - P_r/P_{no}\right) & \text{for } P_r/P_{no} > 0.5 \end{cases} \tag{19}$$

For simplicity in design and compatibility with the existing Direct Analysis procedure for steel members, it is beneficial to maintain the $0.8\tau_b$ factor and have differences in rigidity between steel and composite members manifest only in $EI_{elastic}$. There are several important considerations in the determination of an appropriate value of $EI_{elasitc}$. Even at loading levels below typical service load levels (e.g., those identified in Figure 4), this rigidity must account for the cracking and initial damage that accrues in the member at under combined axial load and bending moment. Additional load-based terms (beyond τ_b) in the expression for EI_{DA} (e.g., as seen in Eqs. 10-11 for a possible variation on $EI_{elastic}$) would be cumbersome and thus load-independent expressions roughly representative of $EI_{elastic}$ for members with high-moment low-axial service loads were selected. It is also important that the ratio of EI_{eff} to EI_{DA} is approximately equal to $0.877\phi_c$ for slender members in certain configurations so that the axial strength is not overestimated when performing the Direct Analysis method (Surovek-Maleck and White 2004a). A proposed expression for $EI_{elastic}$ for use with the Direct Analysis method is given by Eq. 20 for SRCs and Eq. 21 for CFTs. The factors C_1 and C_3 are the same as those in computation of EI_{eff} and are given in Eq. 17 and 4 respectively. The validity of this expression for use in the Direct Analysis method is confirmed though the comparisons presented later in this section. It is likely that this expression is also valid for other purposes (e.g., those described in Section 1) but comprehensive studies have not been performed to confirm such a wide applicability.

$$EI_{elastic} = E_s I_s + E_s I_{sr} + 0.75 C_1 E_c I_c \qquad \text{(SRC)} \tag{20}$$

$$EI_{elastic} = E_s I_s + 0.75 C_3 E_c I_c \qquad \text{(CFT)} \tag{21}$$

Initial imperfections can either be directly modeled (as was done in the fully nonlinear analyses) or represented with notional loads. For these comparisons the notional load approach was used in the design methodology, applying an additional lateral load of 0.2% of the vertical load in each analysis.

6.2 Calculation of Available Strength

The commentary of the AISC *Specification* describes a method of determining the design interaction curve based on the plastic stress distribution method. Three specific points on the section interaction diagram are computed: Point A, the pure axial strength; Point B, the pure bending strength; and Point C, a point with combined loading where the moment is equal to the pure bending strength. The axial strength of each of these points is then reduced by a factor $\chi = P_n/P_{no}$ to obtain the beam-column interaction diagram (Figure 8a). For the Direct Analysis method, P_n is computed using $K=1$.

The commentary methodology performs well for short and moderate length columns; however, it becomes less accurate for slender and concrete dominant columns, where the applied load interaction curve is noticeably concave. Proposed modifications to this methodology are illustrated in Figure 8b. The same section strength is used as the basis, but points C and B are moved inward by factors that depend on the slenderness. The factor α_c (Eq. 22) ranges from P_C/P_A for stocky columns, resulting in the same axial load for point C as in the existing method, and 0.2 for slender columns, resulting in an interaction diagram equivalent to that for structural steel columns (AISC 2010b). The factor α_B (Eq. 23) is not meant to represent a physical reduction in the flexural strength but rather it is a practical option for accounting for the low axial strength of slender columns under large bending loads where the rigidity is severely reduced due to concrete cracking.

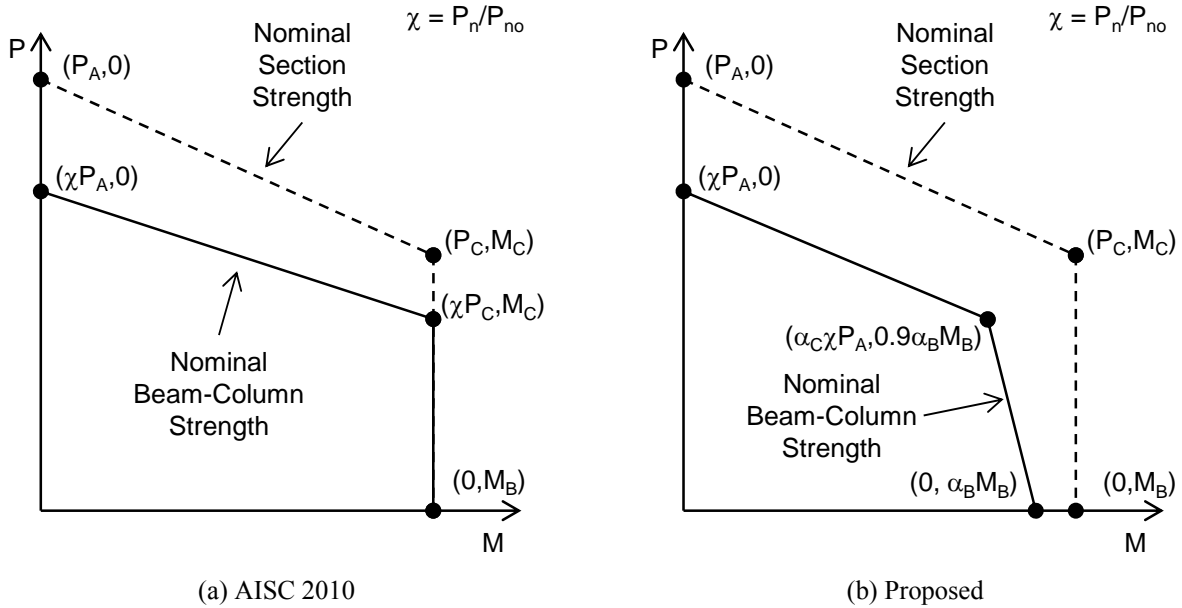(a) AISC 2010   (b) Proposed

Figure 8: Computation of the Design Strength Interaction

$$\alpha_C = \begin{cases} P_C/P_A & \text{for } \lambda_{oe} \leq 0.5 \\ P_C/P_A - (P_C/P_A - 0.2)(\lambda_{oe} - 0.5) & \text{for } 0.5 < \lambda_{oe} \leq 1.5 \\ 0.2 & \text{for } \lambda_{oe} > 1.5 \end{cases} \qquad (22)$$

$$\alpha_B = \begin{cases} 1 & \text{for } \lambda_{oe} \leq 1 \\ 1 - 0.2(\lambda_{oe} - 1) & \text{for } 1 < \lambda_{oe} \leq 2 \\ 0.8 & \text{for } \lambda_{oe} > 2 \end{cases} \tag{23}$$

6.3 Evaluation of the Proposed Design Methodology

To evaluate the validity of the proposed beam-column design methodology, interaction diagrams based on the proposed recommendations are constructed. Sample results for two RCFT sections and one frame are shown in Figure 9 along with the interaction diagrams from the fully nonlinear analyses (blue lines) as described in Section 3.3. The second-order internal force interaction diagram (green dashed lines) is constructed directly from the design equations (Figure 8b). The first-order applied load interaction diagram (green solid lines) is constructed by determining the applied loads that, when applied in a second-order elastic analysis with stiffness reduction (Eqs. 18-21) and notional load, result in peak internal forces that lay on the internal force interaction diagram. The comparisons are performed at the nominal strength level and thus neither resistance factors nor safety factors were used in the computation of the interaction diagrams.
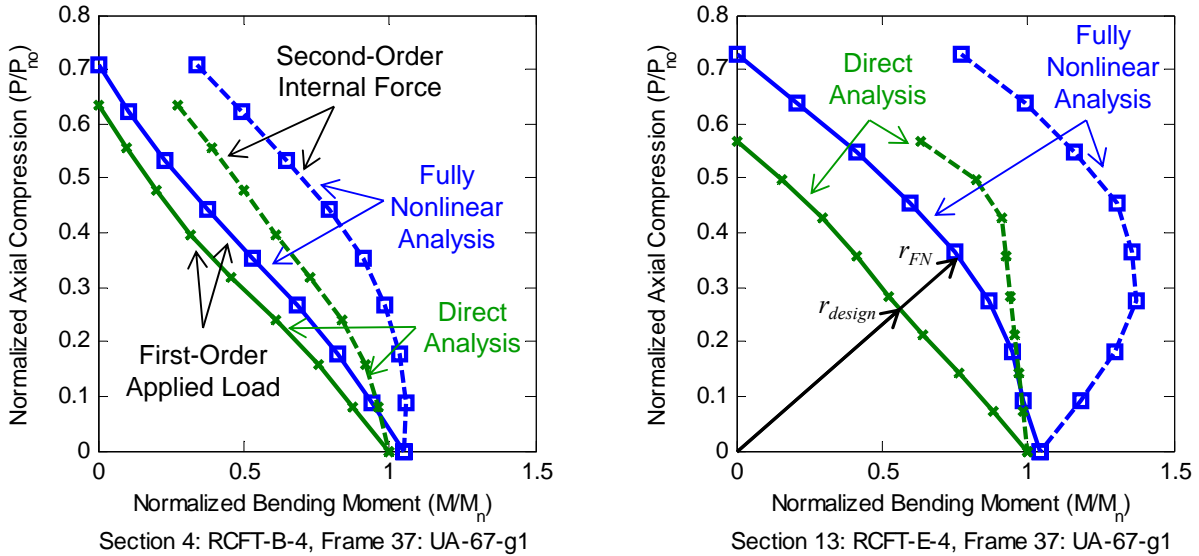

Figure 9: Example Results: Fully Nonlinear and Design Applied Load and Internal Force Interaction Diagrams

Error is computed between the fully nonlinear analysis interaction diagrams and the Direct Analysis interaction diagrams using a radial measure (Eq. 24), where r_{FN} is the distance from the origin to the interaction diagram constructed from the fully nonlinear analyses and r_{design} is the distance along the same line to the interaction diagram constructed from the design methodology. For the first-order applied load interaction diagram unconservative error is negative (e.g., when the green curve lies outside the blue curve in Figure 9).

$$\varepsilon = \frac{r_{FN} - r_{design}}{r_{FN}} \tag{24}$$

Using the radial error, interaction diagrams for different pairs of sections and frames can be compared. An example of this is shown in Figure 10 where the design applied load interaction diagrams for the two RCFT sections shown previously and all 84 frames are compared. The black line (a circle with a radius of one) represents the applied load interaction diagram from the fully nonlinear analyses. The colored lines were constructed by computing the error (Eq. 24) for a sweep of angles and for the same angles plotting points with a distance of $1 - \varepsilon$ from the origin. The colors correspond to the effective length factor of the frame. A colored line outside the black line represents unconservative error and 5% unconservative error is noted by the red dashed line.

In Figure 10, the effect of the effective length factor on the accuracy of the design methodology for these particular cross sections can be seen. Frames with low effective length factors (cyan lines) tend to be more conservative while frames with high effective length factors (magenta lines) tend to be less conservative. For the more concrete dominant section (Figure 10b) the frames with high effective length factors are significantly (greater than 5%) unconservative. In the Direct Analyses, the effective length factor is never computed and thus it is difficult to properly account for these extreme cases without being unduly conservative in more common cases.
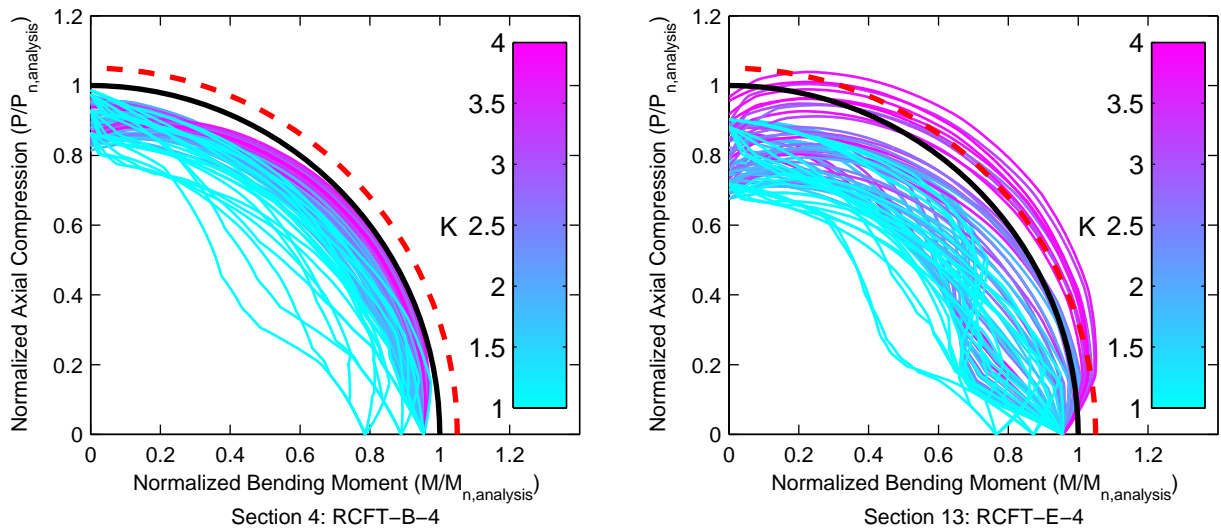

Figure 10: Example Results: Normalized Fully Nonlinear and Design Applied Load Interaction Diagrams

Histograms for each section type showing the relative frequency of the radial error from the first-order applied load interaction diagrams from all sections and frames and through a sweep of angles are shown in Figure 11. A total of 84 (frames) × 15 (sections) = 1,260 sets of interaction diagrams are generated each for RCFTs and CCFTs, and 84 (frames) × 36 (sections) = 3,024 sets of interaction diagrams are generated each for strong and weak axis bending of SRCs. The vertical dashed line indicates the median error, which varies between 11% and 18% conservative (shown as positive in the figure) for each section type. A maximum of 5% unconservative error is desired (ASCE 1997). The proposed design methodology achieves this for most cases. Exceptions are:

- Members with high effective length factors (e.g., an effective length factor, *K*, greater than approximately 3)

- Steel dominant CCFT members where the axial compressive strength, P_n, is overpredicted by the design equations
- Steel dominant weak axis SRC members where the flexural strength, M_n, is overpredicted by the design equations
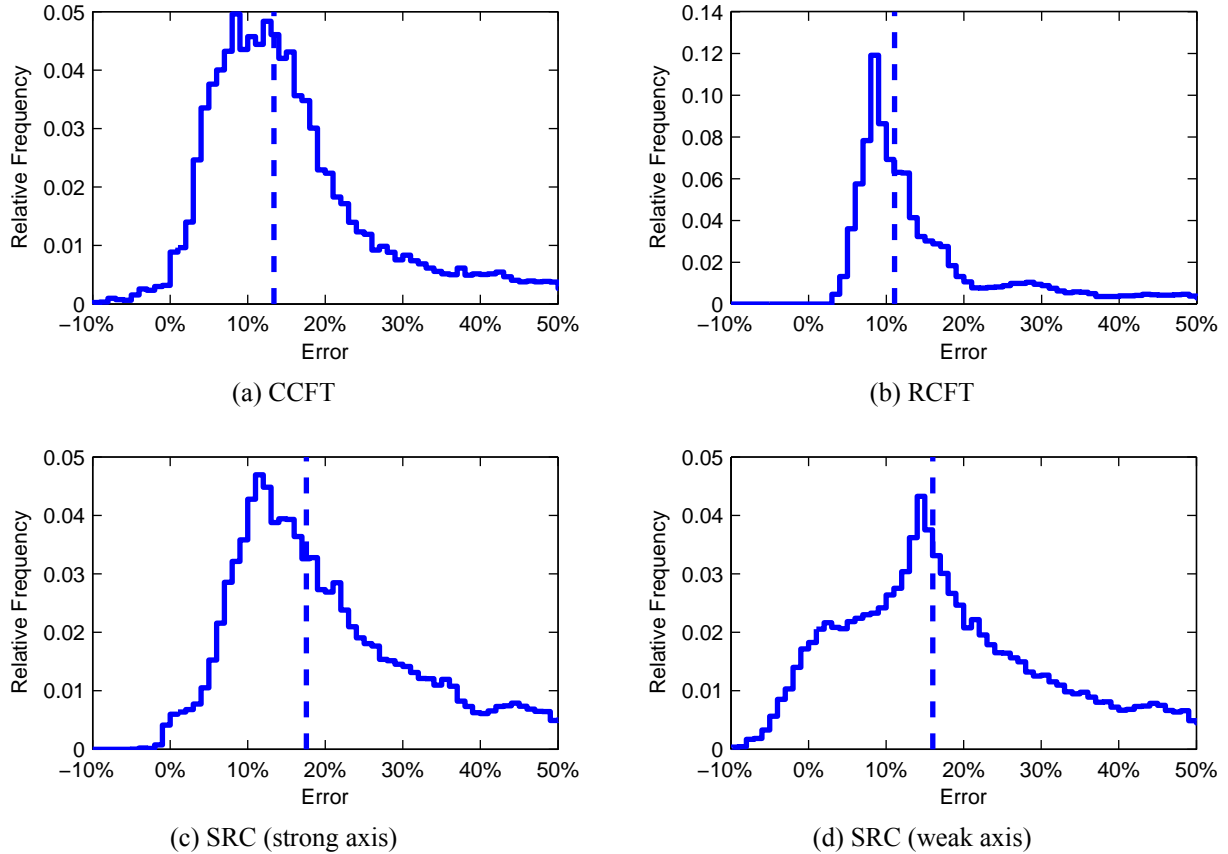

(a) CCFT

(b) RCFT

(c) SRC (strong axis)

(d) SRC (weak axis)

Figure 11: Summary Error Statistics

7. Conclusions

This paper presents the results of a large parametric study undertaken to assess the in-plane stability behavior of steel-concrete composite members, evaluate current design provisions, and develop and validate new design recommendations. This research has developed new elastic flexural rigidities for elastic analysis of composite members; new effective flexural rigidities for calculating the axial compressive strength of SRC members; new Direct Analysis stiffness reductions for composite members; and new recommendations for the construction of the interaction diagram for composite members. The proposed beam-column design methodology is safe and accurate for the vast majority of common cases of composite member behavior, although further research is recommended to continue to investigate the axial compressive strength of steel dominant CCFTs, the weak axis flexural strength of steel dominant SRCs, and members with very high effective length factors, so as to improve the recommendations.

Acknowledgments

References

Abdel-Rahman, N., and Sivakumaran, K. S. (1997). "Material Properties Models for Analysis of Cold-Formed Steel Members." *Journal of Structural Engineering*, ASCE, 123(9), 1135–1143.

AISC. (2010a). *Code of Standard Practice for Steel Buildings and Bridges*. American Institute of Steel Construction, Chicago, Illinois.

AISC. (2010b). *Specification for Structural Steel Buildings*. American Institute of Steel Construction, Chicago, Illinois.

Anslijn, R., and Janss, J. (1974). *Le Calcul des Charges Ultimes des Colonnes Métalliques Enrobées de Béton*. Rapport MT 89, C.R.I.F., Brussels, Belgium.

ASCE. (1997). *Effective Length and Notional Load Approaches for Assessing Frame Stability: Implications for American Steel Design*. American Society of Civil Engineers, Reston, Virginia.

Chang, G. A., and Mander, J. B. (1994). *Seismic Energy Based Fatigue Damage Analysis of Bridge Columns: Part I - Evaluation of Seismic Capacity*. National Center for Earthquake Engineering Research, Department of Civil Engineering, State University of New York at Buffalo, Buffalo, New York.

Chen, C., Astaneh-Asl, A., and Mohle, J. P. (1992). "Behavior and design of high strength composite columns." *Structures Congress '92*, ASCE, San Antonio, Texas, 820–823.

Deierlein, G. G. (2003). *Background and Illustrative Examples of Proposed Direct Analysis Method for Stability Design of Moment Frames*. Report to Task Committee 10, American Institute of Steel Construction, Chicago, Illinois.

Denavit, M. D., and Hajjar, J. F. (2012). "Nonlinear Seismic Analysis of Circular Concrete-Filled Steel Tube Members and Frames." *Journal of Structural Engineering*, ASCE, in press.

Denavit, M. D., Hajjar, J. F., and Leon, R. T. (2011). "Seismic Behavior of Steel Reinforced Concrete Beam-Columns and Frames." *Proceedings of the ASCE/SEI Structures Congress*, ASCE, Las Vegas, Nevada.

Galambos, T. V., and Ketter, R. L. (1959). "Columns under Combined Bending and Thrust." *Journal of Engineering Mechanics Division*, ASCE, 85(2), 135–152.

Hajjar, J. F. (2002). "Composite Steel and Concrete Structural Systems for Seismic Engineering." *Journal of Constructional Steel Research*, 58(5-8), 703–723.

Han, D. J., and Kim, K. S. (1995). "A Study on the Strength and Hysteretic Characteristics of Steel Reinforced Concrete Columns." *Journal of the Architectural Institute of Korea*, 11(4), 183–190.

Han, D. J., Kim, P. J., and Kim, K. S. (1992). "The Influence of Hoop Bar on the Compressive Strength of Short Steel Reinforced Concrete Columns." *Journal of the Architectural Institute of Korea*, 12(1), 335–338.

Kanchanalai, T. (1977). *The Design and Behavior of Beam-Columns in Unbraced Steel Frames*. CESRL Report No. 77-2, Structures Research Laboratory, Department of Civil Engineering, The University of Texas at Austin, Austin, Texas.

Khuntia, M., and Ghosh, S. K. (2004). "Flexural Stiffness of Reinforced Concrete Columns and Beams: Analytical Approach." *ACI Structural Journal*, 101(3), 351–363.

Leon, R. T., Kim, D. K., and Hajjar, J. F. (2007). "Limit State Response of Composite Columns and Beam-Columns Part 1: Formulation of Design Provisions for the 2005 AISC Specification." *Engineering Journal*, AISC, 44(4), 341–358.

Martinez-Garcia, J. M. (2002). "Benchmark Studies to Evaluate New Provisions for Frame Stability Using Second-Order Analysis." Master's Thesis, Department of Civil and Environmental Engineering, Bucknell University, Lewisburg, Pennsylvania.

McKenna, F., Fenves, G. L., and Scott, M. H. (2000). *Open System for Earthquake Engineering Simulation*. Department of Civil and Environmental Engineering, University of California, Berkeley, Berkeley, California.

Perea, T. (2010). "Analytical and Experimental Study on Slender Concrete-Filled Steel Tube Columns and Beam-Columns." Ph.D. Dissertation, School of Civil and Environmental Engineering, Georgia Institute of Technology, Atlanta, Georgia.

Ravindra, M. K., and Galambos, T. V. (1978). "Load and Resistance Factor Design for Steel." *Journal of the Structural Division*, ASCE, 104(9), 1337–1353.

Roderick, J. W., and Loke, Y. O. (1975). "Pin-Ended Composite Columns Bent About the Minor Axis." *Civil Engineering Transactions*, 17(2), 51–58.

Surovek-Maleck, A. E., and White, D. W. (2004a). "Alternative Approaches for Elastic Analysis and Design of Steel Frames. I: Overview." *Journal of Structural Engineering*, ASCE, 130(8), 1186–1196.

Surovek-Maleck, A. E., and White, D. W. (2004b). "Alternative Approaches for Elastic Analysis and Design of Steel Frames. II: Verification Studies." *Journal of Structural Engineering*, ASCE, 130(8), 1197–1205.

Tort, C., and Hajjar, J. F. (2010). "Mixed Finite-Element Modeling of Rectangular Concrete-Filled Steel Tube Members and Frames under Static and Dynamic Loads." *Journal of Structural Engineering*, ASCE, 136(6), 654–664.

White, D. W., Surovek, A. E., Alemdar, B. N., Chang, C. J., Kim, Y. D., and Kuchenbecker, G. H. (2006). "Stability Analysis and Design of Steel Building Frames Using the 2005 AISC Specification." *Steel Structures*, 6, 71–91.